Joint Effects of Void Region Size and Sink Architecture on Underwater WSNs Lifetime

Huseyin Ugur Yildiz, *Senior Member, IEEE*

***Abstract*— Underwater wireless sensor networks (UWSNs) typically suffer from the communication void region problem. A common method to handle the void region problem is to re-route the packets around the void regions. As the size of the void regions increases, packets require more hops to circumvent the large void regions, resulting in a short network lifetime. On the other hand, the void region problem is more destructive in UWSNs utilizing a single-sink architecture than a multi-sink architecture since nodes consume excessive energy for bypassing the void regions to reach the sink node, which can be positioned in a hard-to-reach area in single-sink UWSNs. In this work, an integer linear programming (ILP) model is developed for maximizing UWSNs lifetime while bypassing the void regions. Solving the ILP model to optimality, the joint impact of the void region size and the sink architecture type on UWSNs lifetime is investigated. The results show that the performance of UWSNs significantly drops as the size of the void region grows such that UWSNs lifetimes shorten by up to 61% as the total void region size is one-quarter of the network size. Moreover, multi-sink UWSNs yield better performance than single-sink UWSNs in the void region problem.**

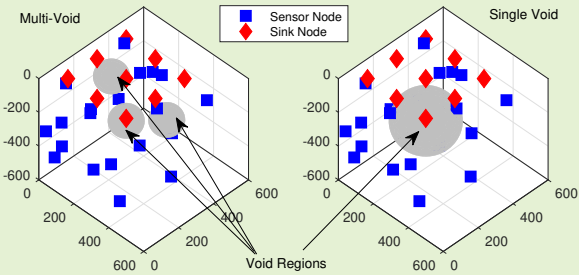

***Index Terms*— underwater wireless sensor networks, communication void region, sink architecture type, integer linear programming, performance evaluation.**

I. Introduction

UNDERWATER Wireless Sensor Networks (UWSNs) are formed by numerous sensor nodes that are randomly deployed in the underwater environment, and at least one sink node (sonobuoy) located at the surface of the water [1]. UWSNs find their place in vast aquatic applications such as military surveillance, marine pollution monitoring, disaster prevention, *etc.* In such applications, sensor nodes monitor and gather information about the environment, and relay the collected data to the destination node(s) [2].

Underwater sensor nodes have scarce battery supplies and limited computational capacity. On the other hand, the underwater environment has characterized by a high bit error rate, long propagation delay, high attenuation due to the noise, *etc.* Battery-operated sensor nodes need to consume high energy to combat the stringent characteristics of the underwater medium [3]. Hence, it is a challenging task to design a routing protocol that optimally balances the energy consumption of sensor nodes for prolonging the operational lifetime of UWSNs [4].

Traditional routing protocols that need to send periodic messages for route discovery and maintenance are impractical for UWSNs since flooding these messages requires excessive energy in the underwater medium [5]. Geographic (localization-based) routing is proven to be a scalable and practical routing technique that can be used for UWSNs as it does not require sending periodic messages for route discovery and maintenance [6]. In geographic routing, each node is aware of its location and forwards the data toward the next-hop node closest to the destination. However, geographic routing suffers from the *communication void region* problem when the current relay node cannot find a next-hop node to forward its packet to the sink node(s) [7]. The common reasons that void regions arise in UWSNs are (i) sparse network topology deployment due to the high cost of sensor nodes, (ii) failure of sensor nodes due to corrosion, fouling, and premature death of nodes, (iii) movement of sensor nodes due to the water current, (iv) obstacles blocking the communication between the nodes (*e.g.*, fish school, ships, *etc.*), and (v) acoustic channel characteristics (*e.g.*, variations in the signal strength) [8]. However, void regions generally occur due to the sparse deployment of high-cost underwater sensor nodes with limited transmission range [9]. Hence, it may not be possible to deploy a high number of underwater sensor nodes to cover the area to be monitored due to the expensive cost of the underwater nodes. In UWSNs, void regions can potentially affect the reliability of the network by disrupting the transmission of acoustic signals. In other words, a void region prevents communication between two or more sensor nodes in the network, forming partitions in the network topology. Since void regions form partitions in the network topology, the connectivity of the network decreases, and packet drops increase [8]. Nevertheless, routing protocols should use recovery methods for creating alternative paths to convey the data to the sink node(s) to handle the void region problem.

Huseyin Ugur Yildiz is with the Department of Electrical and Electronics Engineering, TED University, 06420 Ankara, Turkey (e-mail: hugur.yildiz@tedu.edu.tr)

One of the fundamental recovery methods for the void region problem is to *bypass the void regions* where the aim is to establish routing paths for avoiding the void regions [10]. As the size of void regions increases, packets are routed with more hops to bypass the large void regions, resulting in long delays, high energy dissipation, and consecutively, short lifetimes [11]. On the other hand, single-sink UWSNs have worse performance than multi-sink UWSNs in the void region problem since the number of possible energy-efficient paths from source to destination is smaller for single-sink UWSNs as opposed to multi-sink UWSNs [12]. Furthermore, the difference in the performance between single-sink and multi-sink UWSNs expands as the size of the void regions increases.

Many studies focusing on bypassing the void region strategy in the literature utilize a single sink node over multiple sink nodes. One major disadvantage of using a single sink node in a UWSN consisting of void regions is that sensor nodes have to consume a lot of energy to transmit their data to an ill-positioned remote sink node. Another disadvantage of using a single sink node is that the UWSN lifetime is substantially reduced as the void region size expands. To bypass large void regions, routing paths formed between the sensor nodes and the ill-positioned remote sink node need to have high hop counts (*i.e.*, long routing paths). Considering the two aforementioned disadvantages, the energy consumption of the nodes as well as the overall attenuation will dramatically increase, and the nodes will drain their batteries early, resulting in short UWSN lifetimes. Moreover, the delay experienced on such routing paths with high hop counts can drastically increase, which would have a negative impact on time-critical UWSN applications. On the other hand, the lifetime of UWSN can be extended by adding more sink nodes to the network since it is possible to build energy-efficient and short routing paths (with low hops) between source nodes and a nearby alternative sink node for bypassing the void regions. Currently, the literature does not quantify the amount of change in UWSN lifetime as well as delay, energy efficiency, hop count, and attenuation metrics when the number of sink nodes and the size of void regions jointly vary; hence, we conducted this study in an attempt to fill this gap.

Motivated by the research challenges stated above, the novel contributions of this paper are summarized as follows:

1) We develop an integer linear programming (ILP) formulation for maximizing the UWSNs lifetime. The proposed ILP model finds optimal routing paths from the source node to the destination node(s) in a way of bypassing the void regions available in the network while maximizing the lifetime of the most energy-hungry node at the same time. The ILP model also captures the fundamental principles of underwater acoustic communications at both the physical and the link layers. Bypassing the void regions for maximizing the network lifetime via an ILP-based optimization approach has never been done in the literature before.
2) Through the numerical solutions of the ILP model for a wide range of scenarios, we analyze the impact of varying the number and the size of the void regions on UWSNs lifetime. Note that such a comparison under optimum network operation conditions (*e.g.*, the same assumptions, scenarios, *etc.*) within a generic ILP-based optimization framework has never been conducted in the literature. Moreover, delay, energy efficiency, and hop count performance metrics are also examined when UWSNs lifetime is maximized.
3) We provide a comparative analysis of the utilization of single and multiple sinks in the void region problem for the performance metrics mentioned above. This comparison is conducted within our unified framework, which ensures compatibility with optimal conditions. Note that such a systematic investigation has not been closely explored in the literature before.
4) The joint impact of the void region size and the sink architecture type on UWSNs performance (within network lifetime, delay, energy efficiency, hop count, and attenuation perspectives) is extensively assessed for various network parameter configurations.

The organization of this paper is given as follows. In Section II, we present a brief overview of the void avoidance methods for UWSNs. The energy consumption model, the network model, and the ILP framework are introduced in Section III. The quantitative results of our analysis are discussed in Section IV. Our conclusions are provided in Section V.

II. Related Work

In the literature, there is a large volume of published studies on void-handling strategies for routing protocols in UWSNs. [12] provides an overview of the state-of-the-art of void-handling methods in UWSNs. A classification of void-handling strategies available in the UWSNs literature is summarized in Table I.

Void-handling approaches are categorized into three major groups: *bypassing the void region*, *power control*, and *mobility-assisted* [39]. The majority of void-handling strategies for UWSNs utilize the *bypassing the void region* approach (*e.g.*, [4], [6], [9], [13]–[25]), where the objective is to establish alternative paths for packets to be routed around the void region. In the *power control* approach (*e.g.*, [26]–[30]), nodes in the void region increase their transmission powers to extend their communication ranges for finding a next-hop neighbor to forward the packets. In the *mobility-assisted* approach (*e.g.*, [3], [5], [7], [11], [31]–[34]), the idea is to consume some energy to move the nodes inside the void regions to new depth locations for resuming the packet forwarding. In [39], an analytical framework is proposed to evaluate the performance of the aforementioned void-handling strategies in UWSNs. In the literature, the performance of existing void-handling strategies is typically evaluated in terms of delay, energy efficiency, network lifetime, hop count, *etc.*

Various studies have proposed *hybrid* void-handling strategies in the literature where several void-handling techniques are combined. For example, in [1], [36]–[38], *power control* and *mobility-assisted* approaches are combined. In [2], *bypassing the void regions* as well as *power control* techniques are jointly utilized. In [35], void regions are avoided by the

TABLE I: Classification of void-handling approaches available in the UWSNs literature.

Protocols	Void-Handling Strategy	Sink Architecture	Performance Metrics				
			Lifetime	Delay	Energy Eff.	Hop Count	Attenuation
CELR [13]	Bypassing the Void Region	Single-sink	✗	✓	✓	✗	✗
DFR [14]	Bypassing the Void Region	Single-sink	✗	✗	✗	✗	✗
EAVARP [15]	Bypassing the Void Region	Multi-sink	✓	✓	✓	✗	✗
EERVRM [16]	Bypassing the Void Region	Multi-sink	✓	✓	✓	✗	✗
EVA-DBR [17]	Bypassing the Void Region	Multi-sink	✗	✓	✓	✗	✗
Hydrocast [18]	Bypassing the Void Region	Multi-sink	✗	✓	✓	✗	✗
IVAR [6]	Bypassing the Void Region	Single-sink	✗	✗	✗	✓	✗
LVAR [19]	Bypassing the Void Region	Single-sink	✗	✓	✗	✓	✗
OVAR [4], [9]	Bypassing the Void Region	Single-sink	✗	✓	✓	✓	✗
REBAR [20]	Bypassing the Void Region	Single-sink	✓	✗	✗	✗	✗
RLOR [21]	Bypassing the Void Region	Single-sink	✗	✓	✓	✓	✗
RPSOR [22]	Bypassing the Void Region	Multi-sink	✗	✓	✓	✗	✗
VAPR [23]	Bypassing the Void Region	Multi-sink	✗	✓	✓	✗	✗
VBF [24]	Bypassing the Void Region	Single-sink	✗	✓	✓	✗	✗
VBVA [25]	Bypassing the Void Region	Single-sink	✗	✗	✓	✗	✗
AHH-VBF [26]	Power Control	Single-sink	✗	✓	✓	✗	✗
CARP [27]	Power Control	Single-sink	✗	✓	✓	✗	✗
FBR [28]	Power Control	Multi-sink	✗	✓	✓	✗	✗
LF-IEHM [29]	Power Control	Single-sink	✓	✓	✓	✗	✗
NA-TORA [30]	Power Control	Multi-sink	✗	✓	✓	✗	✗
CTC & DTC [11], [31]	Mobility-Assisted	Multi-sink	✗	✓	✓	✗	✗
DCR [5]	Mobility-Assisted	Multi-sink	✗	✓	✓	✗	✗
GEDAR [3], [7]	Mobility-Assisted	Multi-sink	✗	✓	✓	✗	✗
NGF [32]	Mobility-Assisted	Multi-sink	✓	✗	✓	✗	✗
RVPR [33]	Mobility-Assisted	Multi-sink	✗	✗	✓	✗	✗
WDFAD-DBR [34]	Mobility-Assisted	Multi-sink	✗	✓	✓	✗	✗
A-DBR, B-DBR, C-DBR, and CA-DBR [2]	Hybrid	Multi-sink	✓	✓	✓	✗	✗
EG & DA [35]	Hybrid	Single-sink	✓	✗	✓	✗	✗
iDTC & PADTC [1]	Hybrid	Multi-sink	✗	✓	✓	✗	✗
Im-GEDAR & Co-Im-GEDAR [36]	Hybrid	Multi-sink	✗	✓	✓	✗	✗
DA & TPC [37]	Hybrid	Multi-sink	✗	✓	✓	✗	✗
SHORT [38]	Hybrid	Multi-sink	✓	✓	✗	✗	✗
Our Work	Bypassing the Void Region	Multi-sink	✓	✓	✓	✓	✓

joint consideration of *bypassing the void regions* and *mobility-assisted* approaches.

The existing research on void-handling strategies for UWSNs can also be classified according to the sink architecture type that is utilized in the network into two groups: *single-sink* and *multi-sink*. In single-sink architectures (*e.g.*, [4], [6], [9], [13], [14], [19]–[21], [24]–[27], [29], [35]), all sensor nodes convey their packets to a single sink node (unicast traffic). Void regions occur depending on the location of the single sink floating on the surface of the water. On the other hand, in multi-sink architectures (*e.g.*, [1]–[3], [5], [7], [11], [15]–[18], [22], [23], [28], [30]–[34], [36]–[38]), there are many sink nodes available on the surface of the water, and each sensor node conveys its packets to any of the sink nodes (anycast traffic). In multi-sink architectures, the formation of void regions depends on the point of view of the sink nodes. A void region with respect to a sink node may not be considered a void region with respect to another sink node. Hence, multi-sink architectures have the advantage of handling the void region problem over single-sink architectures.

The most related study to our work is presented in [40], where the authors aim to cover the void region as a circle by virtual coordinate mapping and route the packets from source to destination by circumventing the void regions in two-dimensional WSNs. Furthermore, the effects of both void region size and the number of void regions on the performance metrics, such as delay, the average number of hops to reach the sink node, and energy efficiency are investigated. However, that study is performed for two-dimensional terrestrial WSNs, consisting of a single sink, instead of UWSNs. Moreover, the impact of the void region size on the network lifetime is not examined.

In this study, we do not develop a new algorithm for bypassing void regions in UWSNs. Instead, we aim to investigate how void region size and sink architecture types jointly affect the lifetime of UWSNs within a generic optimization (*i.e.*, ILP) framework under optimum operation conditions (*e.g.*, same assumptions, scenarios, *etc.*). The ILP-based optimization is an ideal way of abstracting the specific details of void-handling techniques described in the literature that may result in suboptimal behavior by removing implementation details which are not relevant to our study.

The reader should bear in mind that this study focuses on *bypassing the void region* strategy (since the majority of void-handling strategies focus on bypassing the void regions), while the *power control* and *mobility-assisted* techniques are beyond the scope of this work. To the best of our knowledge, the impact of void region size (independent of whether there is a single void region or not) on UWSNs lifetime, along with delay, energy efficiency, and hop count performances has never been investigated in the literature. Furthermore, there are no controlled studies that systematically investigate the joint

effects of changing the number of sink nodes and varying the void region size on the performance metrics mentioned above in UWSNs literature.

III. System Model

A. Energy Consumption Model

We follow the principles described in [10], [41] to determine bit and packet error rates for modeling the transmission and energy costs at the link-layer. The acoustic attenuation over the link-(i,j) is calculated as

$$\overline{A_{ij}(f)} = \overline{A_0} + 10\kappa \log_{10}(d_{ij}) + d_{ij} \times 10^{-3} \times \overline{\alpha(f)}, \quad (1)$$

where $\overline{A_0}$, κ, d_{ij}, f, and $\overline{\alpha(f)}$ are the transmission anomaly (in dB), the spreading factor, the link distance (in m), the central operation frequency (in kHz), and the absorption coefficient (in dB/km), respectively. According to Thorp's formula, $\overline{\alpha(f)}$ is defined as

$$\overline{\alpha(f)} = \frac{0.11 f^2}{1+f^2} + \frac{44 f^2}{4100+f^2} + 2.75 \cdot 10^{-4} f^2 + 0.003. \quad (2)$$

The power of the ambient noise (in dB) is approximated as

$$\overline{N(f)} \approx 50 - 18 \log_{10}(f). \quad (3)$$

The received signal-to-noise ratio (SNR – in dB) is calculated according to the passive sonar equation as

$$\overline{\gamma_{ij}(f)} = \overline{\mathrm{SL}} - \overline{N(f)} - \overline{A_{ij}(f)}, \quad (4)$$

where $\overline{\mathrm{SL}}$ is the acoustic transmission power (in dB re 1μPa), which is given as

$$\overline{\mathrm{SL}} = 10 \log_{10} \left(\frac{P_{\mathrm{tx}}}{2\pi H I_0} \right). \quad (5)$$

In this expression, P_{tx}, $I_0 = 0.67 \times 10^{-18}$, and H are the transmit power (in W), the intensity of the transmitted signal, and the depth of the water (in m), respectively. By employing the binary phase-shift keying (BPSK) modulation, the bit error rate (BER) is expressed as

$$p_{ij}^b = \frac{1}{2} - \frac{1}{2} \sqrt{\frac{10^{\overline{\gamma_{ij}(f)}/10}}{1 + 10^{\overline{\gamma_{ij}(f)}/10}}}. \quad (6)$$

For the sake of readability, we omit the f notation in p_{ij}^b. A packet of size q bits transmitted from node-i is successfully received at node-j with the probability

$$p_{ij}^S(q) = (1 - p_{ij}^b)^q. \quad (7)$$

We employ a slotted automatic-repeat-request (ARQ) communication scheme to guarantee packet transmission [18]. In each slot, the transmitter node-i sends a data packet of l_d bits to the receiver node-j. Node-i remains in idle sensing mode once the data transmission is complete, waiting for an acknowledgment (ACK) packet. On the other hand, the receiver node-j stays in idle mode to wait for the data packet transmitted by node-i. As the data packet is successfully received at the receiver node-j, an ACK packet of size l_a bits is transmitted back to node-i. Hence, the ARQ slot time in the link-(i,j) is calculated as

$$t_{ij}^{\mathrm{slot}} = \frac{l_d}{R} + 2 \times \frac{d_{ij}}{c} + \frac{l_a}{R}, \quad (8)$$

where R, $2 \times \frac{d_{ij}}{c}$, and c are the bit rate (in bps), the two-way propagation delay (in seconds), and the speed of sound in underwater (in seconds), respectively. A node stays in idle sensing mode for at least $2 \times \frac{d_{ij}}{c}$ seconds independent of packet errors. Retransmission is required whenever the handshake is not successful. Hence, the mean number of transmissions needed to complete a handshake cycle is defined as

$$n_{ij}^{\mathrm{ret}} = \left[p_{ij}^S(l_d) \times p_{ji}^S(l_a) \right]^{-1}, \quad (9)$$

where $p_{ij}^S(l_d)$ and $p_{ji}^S(l_a)$ are probabilities to successfully receive a data packet (of size l_d bits) and an ACK packet (of size l_a bits), respectively. The transmission energy cost for this slotted ARQ scheme is expressed as

$$E_{ij}^{\mathrm{tx}} = \frac{1 - p_{ij}^S(l_d) p_{ji}^S(l_a)}{\left(n_{ij}^{\mathrm{ret}}\right)^{-1}} \left[P_{\mathrm{tx}} \frac{l_d}{R} + P_{\mathrm{idle}} \left(t_{ij}^{\mathrm{slot}} - \frac{l_d}{R} \right) \right] + \frac{p_{ij}^S(l_d) p_{ji}^S(l_a)}{\left(n_{ij}^{\mathrm{ret}}\right)^{-1}} \left[P_{\mathrm{tx}} \frac{l_d}{R} + P_{\mathrm{rx}} \frac{l_a}{R} + P_{\mathrm{idle}} \left(t_{ij}^{\mathrm{slot}} - \frac{l_d}{R} - \frac{l_a}{R} \right) \right]. \quad (10)$$

The first term in Eq. (10) represents the energy cost for the unsuccessful handshake case, while the second term models the energy cost for the successful handshake case. Note that P_{rx} and P_{idle} are the powers required for reception and staying in idle mode (in W). Similarly, the reception energy cost for the slotted ARQ scheme is presented as

$$E_{ji}^{\mathrm{rx}} = \frac{1 - p_{ij}^S(l_d)}{\left(n_{ij}^{\mathrm{ret}}\right)^{-1}} \left[P_{\mathrm{idle}} \times t_{ij}^{\mathrm{slot}} \right] + \frac{p_{ij}^S(l_d)}{\left(n_{ij}^{\mathrm{ret}}\right)^{-1}} \times \left[P_{\mathrm{tx}} \frac{l_a}{R} + P_{\mathrm{rx}} \frac{l_d}{R} + P_{\mathrm{idle}} \left(t_{ij}^{\mathrm{slot}} - \frac{l_d}{R} - \frac{l_a}{R} \right) \right]. \quad (11)$$

In this notation, the first and the second terms model the energy dissipation costs for the unsuccessful and successful handshake cases.

B. Network Model

We consider a static three-dimensional UWSN that consists of $|N_N|$ number of ordinary sensor nodes and $|N_S|$ number of surface sink nodes, where N_N and N_S are the sets of sensor and sink nodes, respectively. Moreover, $N = N_N \cup N_S$ is defined to be the set of all nodes in the network. All ordinary sensor nodes have initial battery energy of E_{bat} (in J), and sink nodes are assumed to have no constraints on the battery energy [1]. Ordinary sensor nodes are randomly deployed in a cubic volume with an edge size of d_{net} m. Each node has a transmission range of R_{comm} m. The sink nodes are deployed in a pre-determined manner as in [39] such that the surface of the water (which has a size of d_{net}^2 m^2) is partitioned into $|N_S|$ number of equal-sized squares, where each sink node is placed on the center of these small squares. Each sensor node is assumed to know both its location and the location of the sink nodes [26].

The operational time of the network is divided into *rounds*, where each round lasts T_{rnd} seconds. The network lifetime is defined as the number of rounds until the first node depletes its initial battery energy [20]. We define L_{rnd} to represent the network lifetime in terms of rounds. Hence, the network

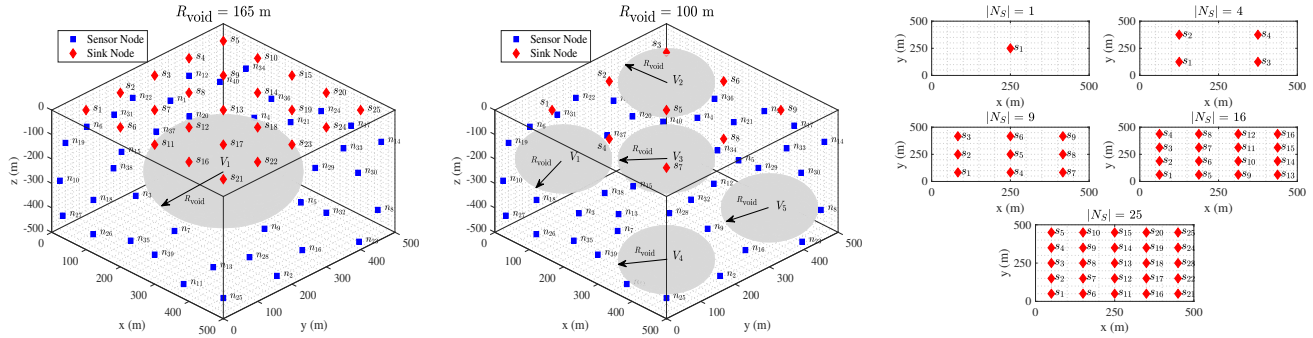

(a) Single Void (SV) (b) Multi-Void (MV) (c) Sink Deployment

Fig. 1: Illustrations of single void (a) and multi-void (b) scenarios for a 40-node UWSN with 25 surface sink nodes, where $\varphi = V_{\text{void}}/V_{\text{net}} = 0.15$. The deployment of surface sink nodes is presented in (c).

lifetime is represented as $L_{\text{rnd}} \times T_{\text{rnd}}$ in seconds. Each sensor node-i generates s_i number of data packets of size l_d bits in each round, and the generated data by these nodes are collected at any of the sink nodes. We assume that if a data packet is terminated at any of the sink nodes, the transmission is considered successful [2].

The impact of void region size on UWSNs performance is investigated by considering two scenarios [40]. In both scenarios, the void region is described as a spherical region without any nodes inside the sphere [9]. In the first scenario (*single void* – SV), we consider a single void region centered in the middle of the network and has a radius of R_{void} (in m). We investigate the changes in UWSNs performance by varying R_{void}. In the second scenario (*multi-void* – MV), we randomly generate the center coordinates of multiple non-intersecting void regions with fixed radii ($R_{\text{void}} = 100$ m). In this case, we observe the differences in UWSNs performance by varying the number of void regions. In both scenarios, φ is defined as the ratio of the total volume of the void regions to the volume of the network (*i.e.*, $\varphi = V_{\text{void}}/V_{\text{net}}$) for quantitatively exploring the impact of void region size on UWSNs performance.

We illustrate SV and MV scenarios on UWSNs consisting of 40 ordinary sensor nodes (*i.e.*, $|N_N| = 40$) and 25 surface sink nodes (*i.e.*, $|N_S| = 25$) in Figs. 1a and 1b, respectively. In these figures, sensor nodes, surface sink nodes, and void regions are denoted by $\{n_1, n_2, \ldots, n_{40}\}$, $\{s_1, s_2, \ldots, s_{25}\}$, and $\{V_1, V_2, \ldots, V_5\}$, respectively. We set $d_{\text{net}} = 500$ m, and the volume of the UWSN is calculated as $V_{\text{net}} = d_{\text{net}}^3 = 125 \times 10^6$ m^3. For this network model, the total volume of the void regions is assumed to be 15% of the volume of the UWSN (*i.e.*, $\varphi = V_{\text{void}}/V_{\text{net}} = 0.15$). For the SV scenario (in Fig. 1a), a single spherical void region (*i.e.*, V_1) is centered in the middle of the network, which has the volume $V_{\text{void}} = V_{\text{net}} \times \varphi = \frac{4}{3}\pi R_{\text{void}}^3 = 18.75 \times 10^6$ m^3. Therefore, the single void region has a radius of $R_{\text{void}} = \sqrt[3]{\frac{3 \times V_{\text{void}}}{4\pi}} = \sqrt[3]{\frac{3 \times 18.75 \times 10^6}{4\pi}} \approx 165$ m. For the MV scenario (in Fig. 1b), we have multiple void regions each having a radius of $R_{\text{void}} = 100$ m and volume of $V_{\text{void}} = \frac{4}{3}\pi R_{\text{void}}^3 = 4.19 \times 10^6$ m^3. Therefore, we need to have $\lceil \frac{\varphi \times V_{\text{net}}}{V_{\text{void}}} \rceil = \lceil \frac{0.15 \times 125 \times 10^6}{4.19 \times 10^6} \rceil = \lceil 4.47 \rceil = 5$ void regions in the UWSN such that $\varphi \approx 0.15$. Finally, Fig. 1c shows surface sink deployment for the single-sink (*i.e.*, $|N_S| = 1$) and multi-sink architectures (*i.e.*, $|N_S| > 1$).

C. The ILP Model For Maximizing UWSNs Lifetime

The ILP model that maximizes the UWSNs lifetime while bypassing the void regions is presented in (12). The ILP model is formulated as a MaxMin problem (*i.e.*, maximizing the lifetime of the node having the minimum lifetime) [42]. In this way, all sensor nodes work together to prevent premature death of nodes by dissipating their battery energies evenly. The decision variables of the ILP model are denoted by the integer variables: x_{ij}^k and $\mathcal{H}_i^k$. x_{ij}^k is the number of flows (packets) produced by sensor node-k flowing over the link-(i,j) through the network lifetime. $\mathcal{H}_i^k$ is the number of flows produced by sensor node-k that is gathered at the sink node-i during the network lifetime. The objective function of the ILP model is defined in (12a), which aims to maximize the number of rounds that UWSN can operate (L_{rnd}). The constraints of the ILP model are stated in (12b)–(12k).

$$\text{Maximize } L_{\text{rnd}} \tag{12a}$$

subject to:

$$\sum_{\substack{j \in N \\ i \neq j}} x_{ij}^k - \sum_{\substack{j \in N_N \\ i \neq j}} x_{ji}^k = \begin{cases} s_k \times L_{\text{rnd}} & \text{if } i = k \\ 0 & \text{o.w.} \end{cases}, \quad \forall i, k \in N_N \tag{12b}$$

$$\sum_{\substack{j \in N \\ i \neq j}} x_{ij}^k - \sum_{\substack{j \in N_N \\ i \neq j}} x_{ji}^k = -\mathcal{H}_i^k, \quad \forall i \in N_S, \forall k \in N_N \tag{12c}$$

$$\sum_{j \in N_N} x_{jk}^k = 0, \quad \forall k \in N_N \tag{12d}$$

$$\sum_{j \in N} x_{kj}^k = 0, \quad \forall k \in N_S \tag{12e}$$

$$\sum_{k \in N_N} \sum_{i \in N_S} \mathcal{H}_i^k = \left(\sum_{i \in N_N} s_i \right) \times L_{\text{rnd}} \tag{12f}$$

$$\sum_{k\in N_N}\left(\sum_{j\in N} x_{ij}^k n_{ij}^{\text{ret}} t_{ij}^{\text{slot}} + \sum_{j\in N_N} x_{ji}^k n_{ji}^{\text{ret}} t_{ji}^{\text{slot}}\right) \leq L_{\text{rnd}} \times T_{\text{rnd}}, \quad \forall i \in N \tag{12g}$$

$$\sum_{k\in N_N}\left(\sum_{j\in N} x_{ij}^k E_{ij}^{\text{tx}} + \sum_{j\in N_N} x_{ji}^k E_{ji}^{\text{rx}}\right) \leq E_{\text{bat}}, \quad \forall i \in N_N \tag{12h}$$

$$x_{ij}^k = 0 \text{ if } d_{ij} > R_{\text{comm}} \text{ or } \theta_{ij} = 1, \quad \forall i,k,j \in N \tag{12i}$$

$$x_{ij}^k \geq 0, \quad \forall i,k,j \in N \tag{12j}$$

$$\mathcal{H}_i^k \geq 0, \quad \forall k \in N_N, \forall i \in N_S \tag{12k}$$

Const. (12b) balances the flows at each source node-i ($i = k$), and relay nodes ($i \neq k$, nodes that are neither source nodes nor sink nodes) such that the difference between the summation of outgoing flows ($\sum_{\substack{j\in N \\ i\neq j}} x_{ij}^k$) and the summation of incoming flows ($\sum_{\substack{j\in N_N \\ i\neq j}} x_{ji}^k$) is equal to the total number of generated flows by node-k over the network lifetime ($s_k \times L_{\text{rnd}}$) when $i = k$, or 0 when $i \neq k$. Const. (12c) conserves flows at each sink node-i for each source node-k. The right-hand side of this constraint shows the total number of flows (generated by sensor node-k) collected at each sink node-i through the network lifetime ($\mathcal{H}_i^k$). Const. (12d) is the loop elimination constraint at each source node-k. Const. (12e) prevents flows from being generated by each sink node. Const. (12f) equates the total number of gathered flows at all sink nodes (left-hand side) to the total number of generated flows during the network lifetime (right-hand side). Const. (12g) states that the total communication (transmission and reception) time of each node-i cannot be greater than the network lifetime (in terms of seconds). In this constraint, the parameters t_{ij}^{slot} and n_{ij}^{ret}, are calculated by using Eqs. (8) and (9), respectively. Const. (12h) limits the total energy dissipated for transmission and reception of each sensor node-i during the network lifetime to the initial battery energy (E_{bat}). The parameters, E_{ij}^{tx} and E_{ji}^{rx}, are obtained in Eqs. (10) and (11), respectively. Const. (12i) defines two cases for zero flows. In the first case, if node-i wants to transmit its packet to node-j, which is beyond its transmission range (*i.e.*, $d_{ij} > R_{\text{comm}}$), a zero flow occurs. In the second case, if the transmission between node-i and node-j is intercepted by any of the void regions available in the network, a zero flow also occurs. We define θ_{ij} as a parameter that takes 1 if the direct transmission between node-i and node-j is intercepted by any of the void regions available in the network, and 0, otherwise. We use the methodology presented in [43] to determine θ_{ij} values for a given network topology. Hence, the ILP model finds alternative route paths to bypass the void regions for maximizing the network lifetime. Consts. (12j) and (12k) define the boundaries of the decision variables.

IV. Analysis

In this section, we explore the effects of void region size on UWSNs lifetime by solving the ILP model in (12) to optimality for various network density, sink deployment, and initial power consumption configurations. The other performance metrics; delay, energy efficiency, hop count, and attenuation are also examined when the network lifetime is maximized. The impact of void region size on the performance of UWSNs is investigated via SV and MV scenarios. Moreover, the effects of using single-sink and multi-sink architectures are also considered throughout the analyses. The energy consumption model and the network model are implemented in Python, while the ILP model is solved using the GUROBI solver. The parameters used throughout the analyses are listed in Table II.

TABLE II: Parameters used through the analyses.

Parameter	Description	Value
$\lvert N_N\rvert$	Total number of sensor nodes	{30, 40, 50}
$\lvert N_S\rvert$	Total number of sink nodes	{1, 4, 9, 16, 25}
$\overline{A_0}$	Transmission anomaly	30 dB
c	Speed of sound in underwater	1500 m/s
d_{net}	Edge size of the network	500 m
E_{bat}	Battery energy	1000 J
f	Operation frequency	10 kHz
l_a	ACK packet size	4 bytes
l_d	Data packet size	100 bytes
P_{idle}	Idle sensing power	0.01 W
P_{rx}	Reception power	0.1 W
P_{tx}	Transmission power	{2, 4, 8} W
R	Data rate	50 kbps
R_{comm}	Transmission range	250 m
s_k	Number of data packets generated by node-k at each round	1
T_{rnd}	Round duration	100 s
κ	Spreading factor	2
φ	$V_{\text{void}}/V_{\text{net}}$	0–0.25

We consider five performance metrics:

1) *Absolute Network Lifetime (ANL):* is defined as the number of rounds until the first node depletes its initial battery energy (L_{rnd}).
2) *Average End-to-End Delay (AED):* is defined as the average time (in seconds) required for a single flow to be transmitted from a source node to any of the sink nodes successfully. AED is calculated as $\frac{1}{|N_N|}\left(\sum_{k\in N_N}\sum_{i\in N}\sum_{j\in N}\frac{x_{ij}^k n_{ij}^{\text{ret}} t_{ij}^{\text{slot}}}{s_k \times L_{\text{rnd}}}\right)$.
3) *Average Energy Tax (AET):* is defined as the average energy cost for transmission and reception when a single flow is delivered to any of the sink nodes successfully. AET is calculated as $\frac{1}{|N_N|}\left(\sum_{k\in N_N}\sum_{i\in N}\sum_{j\in N}\frac{x_{ij}^k [E_{ij}^{\text{tx}} + E_{ji}^{\text{rx}}]}{s_k \times L_{\text{rnd}}}\right)$.
4) *Average Hop Count (AHC):* is defined as the average number of hops required for a single flow to be collected at any of the sink nodes successfully. AHC is calculated as $\frac{1}{|N_N|}\left(\sum_{k\in N_N}\sum_{i\in N}\sum_{j\in N}\frac{x_{ij}^k}{s_k \times L_{\text{rnd}}}\right)$.
5) *Accumulated Path Loss (APL):* is defined as the accumulated attenuation (in dB) experienced that a single flow is transmitted from a source node to any of the sink nodes successfully. APL is calculated as $\frac{1}{|N_N|}\left(\sum_{k\in N_N}\sum_{i\in N}\sum_{j\in N}\frac{x_{ij}^k n_{ij}^{\text{ret}} \overline{A_{ij}(f)}}{s_k \times L_{\text{rnd}}}\right)$.

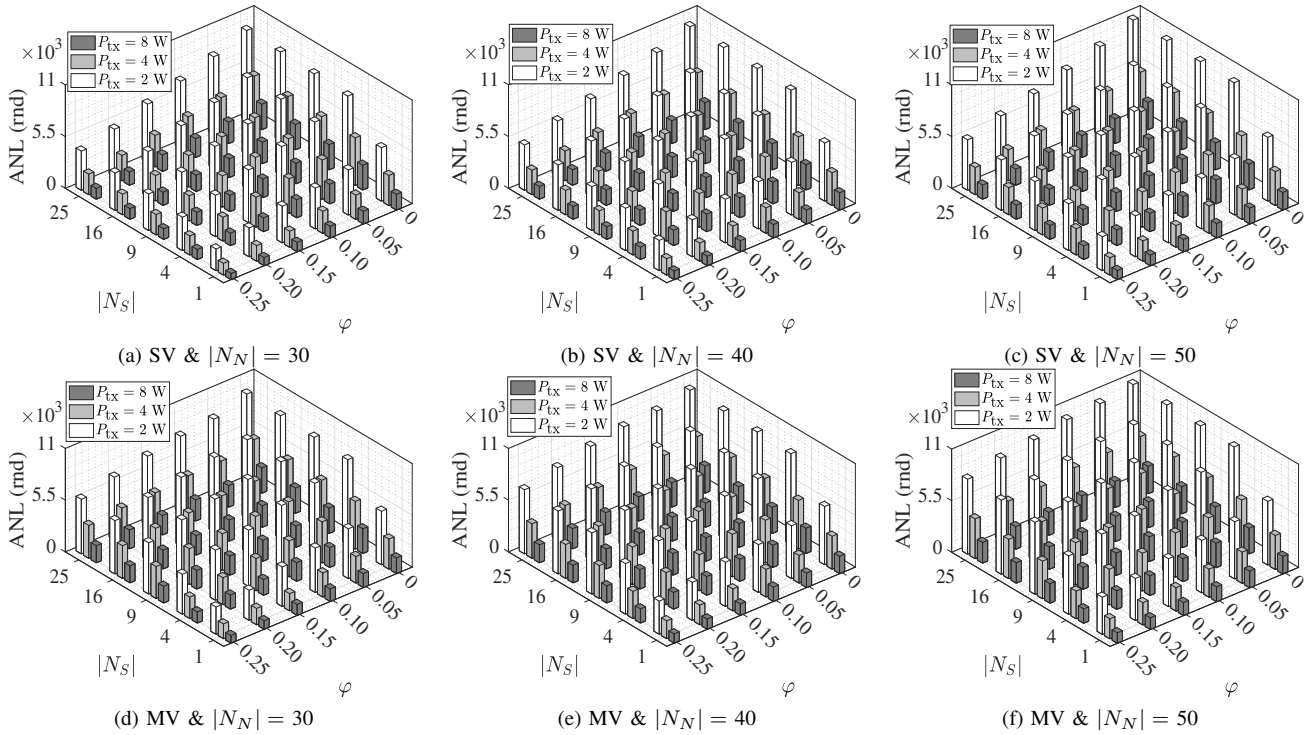

(a) SV & $|N_N| = 30$ (b) SV & $|N_N| = 40$ (c) SV & $|N_N| = 50$

(d) MV & $|N_N| = 30$ (e) MV & $|N_N| = 40$ (f) MV & $|N_N| = 50$

Fig. 2: ANLs (rounds) as a function of φ, $|N_S|$, and P_{tx} for three $|N_N|$ values for the SV and MV scenarios.

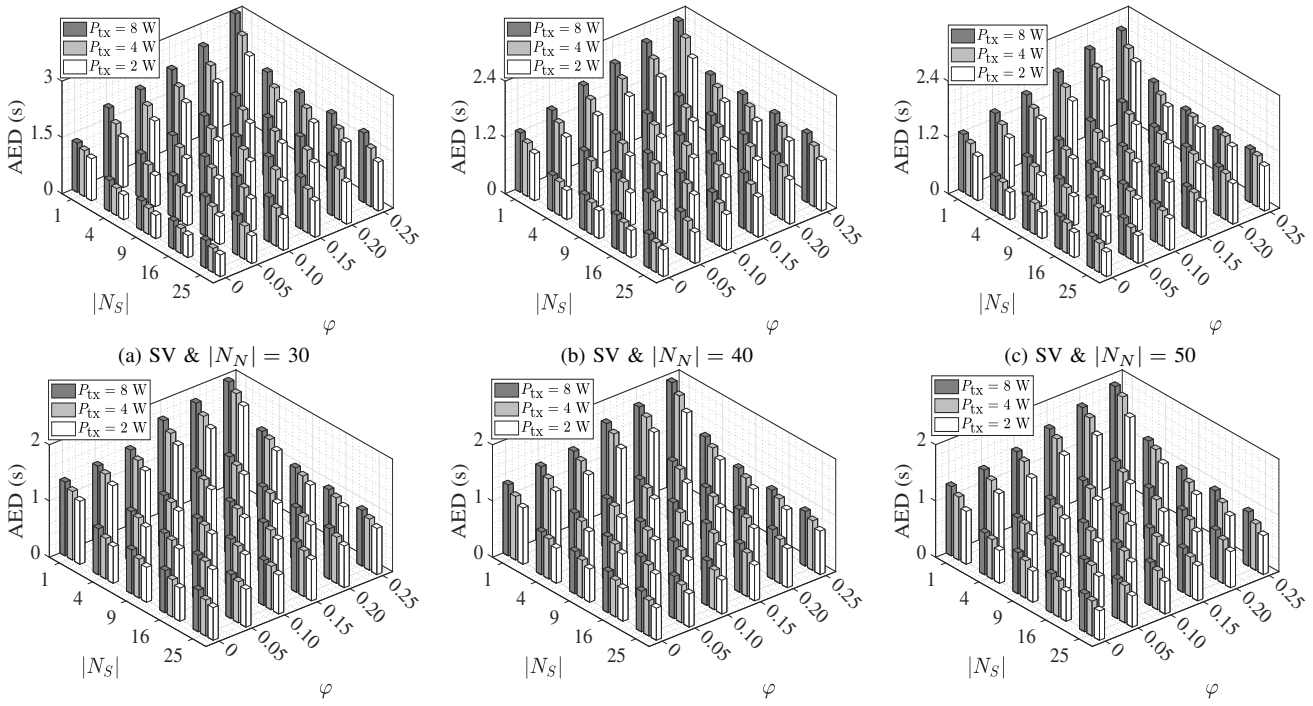

(a) SV & $|N_N| = 30$ (b) SV & $|N_N| = 40$ (c) SV & $|N_N| = 50$

(d) MV & $|N_N| = 30$ (e) MV & $|N_N| = 40$ (f) MV & $|N_N| = 50$

Fig. 3: AEDs (s) as a function of φ, $|N_S|$, and P_{tx} for three $|N_N|$ values for the SV and MV scenarios.

We use the optimal solutions for the decision variables, x_{ij}^k, which maximize L_{rnd} for calculating AED, AET, AHC, and APL performance metrics.

In Figs. 2–6, we use three-dimensional bar plots to present the five performance metrics. Each figure has six sub-figures. In each column, the number of sensor nodes in the UWSN (*i.e.*, $|N_N|$) is changed to examine the effects of the network density on each performance metric. In the top and bottom rows, the results for the SV and MV scenarios are provided, respectively. In the SV scenario (top row), R_{void} is adjusted

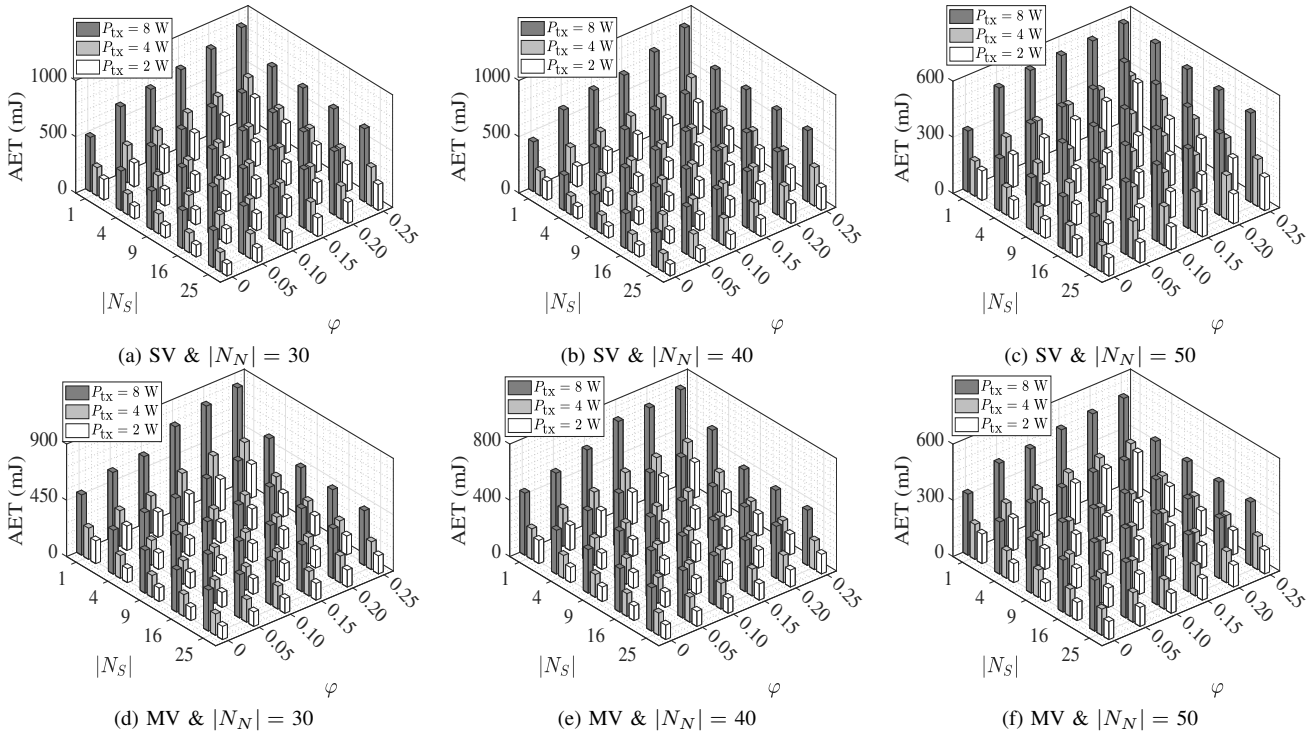

(a) SV & $|N_N| = 30$ (b) SV & $|N_N| = 40$ (c) SV & $|N_N| = 50$

(d) MV & $|N_N| = 30$ (e) MV & $|N_N| = 40$ (f) MV & $|N_N| = 50$

Fig. 4: AETs (mJ) as a function of φ, $|N_S|$, and P_{tx} for three $|N_N|$ values for the SV and MV scenarios.

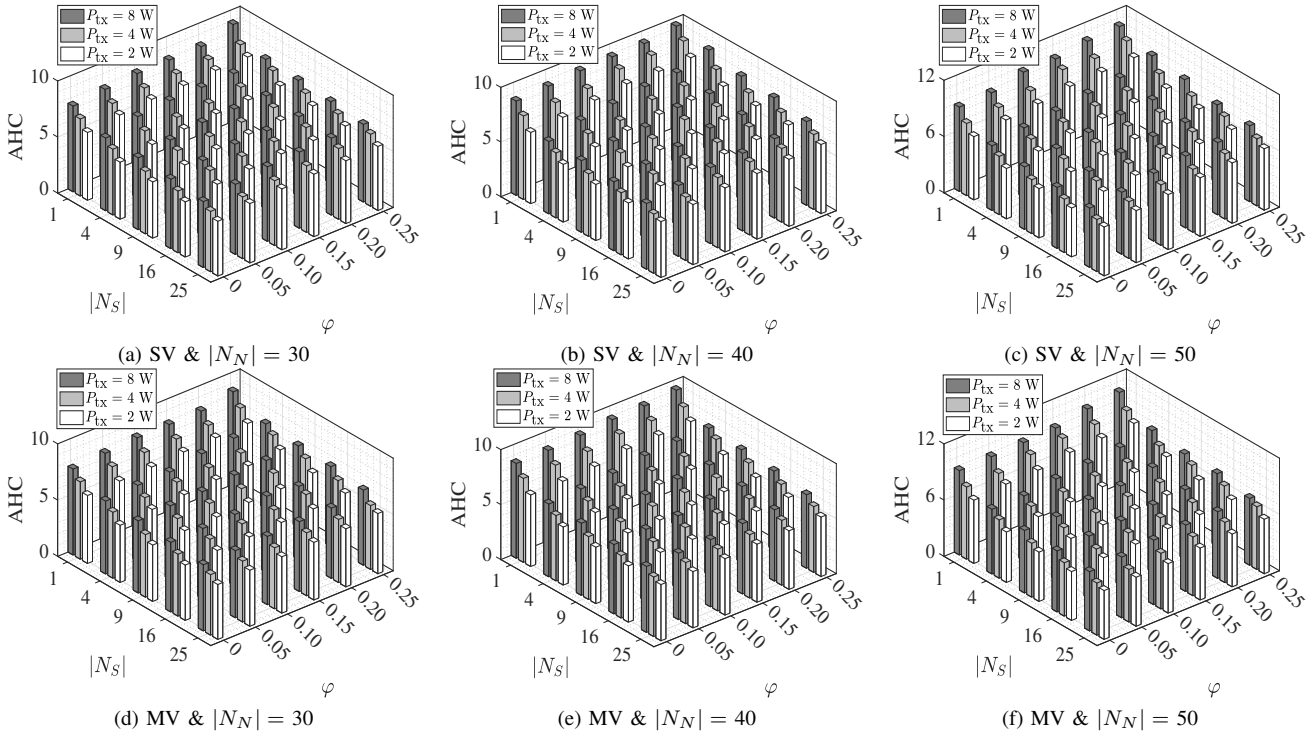

(a) SV & $|N_N| = 30$ (b) SV & $|N_N| = 40$ (c) SV & $|N_N| = 50$

(d) MV & $|N_N| = 30$ (e) MV & $|N_N| = 40$ (f) MV & $|N_N| = 50$

Fig. 5: AHCs as a function of φ, $|N_S|$, and P_{tx} for three $|N_N|$ values for the SV and MV scenarios.

according to the chosen φ value. In the MV scenario (bottom row), we fix $R_{\text{void}} = 100$ m and change the number of void regions according to the picked φ value. The three axes of each sub-figure are explained as follows. In x-axes, the ratio of the total volume of the void regions to the volume of the UWSN (*i.e.*, φ) is varied between 0 and 0.25, with an increment of 0.05. $\varphi = 0$ is considered the baseline case when there are no void regions available in the network. By changing φ values, we analyze the impact of void region size on each performance metric. In y-axes, the number of sink nodes is varied between 1 and 25. $|N_S| = 1$ states that the UWSN has a single sink, while $|N_S| > 1$ corresponds to the multi-

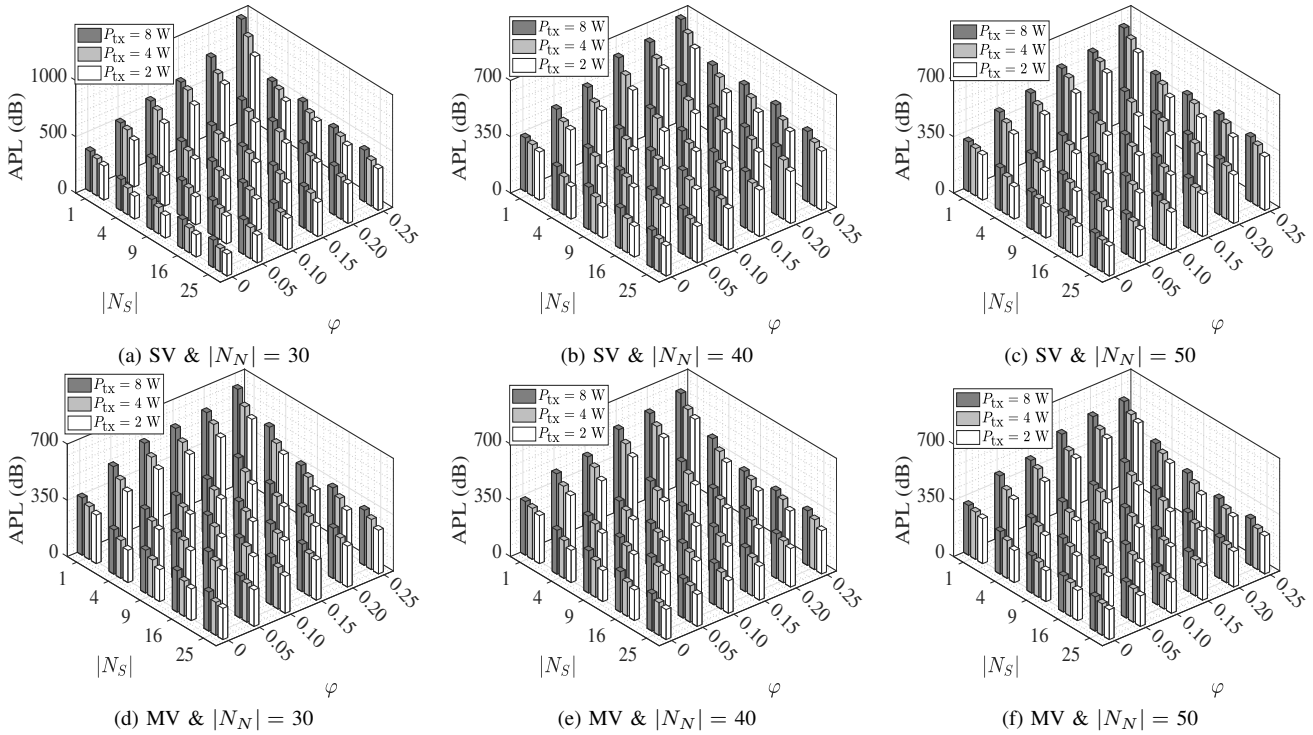

(a) SV & $|N_N| = 30$ (b) SV & $|N_N| = 40$ (c) SV & $|N_N| = 50$

(d) MV & $|N_N| = 30$ (e) MV & $|N_N| = 40$ (f) MV & $|N_N| = 50$

Fig. 6: APLs (dB) as a function of φ, $|N_S|$, and P_{tx} for three $|N_N|$ values for the SV and MV scenarios.

sink architecture. By varying $|N_S|$ values, the effects of sink architecture type on each performance metric are assessed. In z-axes, the performance metric that is examined is given. For fixed φ and $|N_S|$ values, we provide a grouped bar plot consisting of three bars for the three chosen transmission power (*i.e.*, P_{tx}) values (*i.e.*, $P_{\text{tx}} = 2$ W, 4 W, and 8 W [29]), where each bar shows the average values of over 50 randomly generated topologies.

We present ANLs with respect to φ, $|N_S|$, and P_{tx} considering three different network density configurations (*i.e.*, three $|N_N|$ values) for SV and MV scenarios in Fig. 2. $|N_N|$ is set to 30, 40, and 50 for the SV scenario in Figs. 2a, 2b, and 2c, respectively. The results for the MV scenario are given in Figs. 2d, 2e, and 2f. Our results show that ANLs are the highest for multi-sink UWSNs (with $|N_S| = 25$) when there are no void regions in the network (*i.e.*, $\varphi = 0$) for the lowest transmission power (*i.e.*, $P_{\text{tx}} = 2$ W). Regardless of the sink architecture type, network density, and transmission power, SV and MV scenarios yield the same ANLs when $\varphi = 0$. In each sub-figure, ANLs decrease as φ increases for fixed $|N_S|$ and P_{tx} values since sensor nodes need to consume high energy for bypassing the large void regions for conveying data packets to the sink node(s). Moreover, ANLs reduce as P_{tx} increases for constant $|N_S|$ and φ values, since the cost of communication in terms of energy increases as P_{tx} rises. ANLs for the MV scenario are at most 59% greater than the ANLs for the SV scenario since there are more alternative energy-efficient routing paths available in the MV scenario than in the SV scenario. ANLs are observed in the intervals of 2311–10694 rounds (when $P_{\text{tx}} = 2$ W), 1257–5636 rounds (when $P_{\text{tx}} = 4$ W), and 657–2921 rounds (when $P_{\text{tx}} = 8$ W) for the SV scenario. For the MV scenario, ANLs are obtained as 2899–10694, 1572–5636, and 821–2921 rounds for $P_{\text{tx}} = 2$ W, 4 W, and 8 W, respectively. Void-free ANLs (obtained with $\varphi = 0$) drop up to 61% when $\varphi = 0.25$. ANLs get shortened as $|N_S|$ decreases for fixed φ and P_{tx} values since the number of energy-efficient routing paths from source to destination for maximizing the network lifetime reduces as $|N_S|$ decreases. ANLs are the lowest for single-sink UWSNs (*i.e.*, $|N_S| = 1$). Multi-sink UWSNs can increase ANLs of single-sink UWSNs at a minimum of 37%. Nevertheless, ANLs are in the intervals of 657–6790 rounds and 1062–10694 rounds for the single-sink and multi-sink architectures, respectively. Increasing $|N_N|$ helps ANLs be improved since the path lengths decrease as $|N_N|$ grows, resulting in nodes consuming low energy for transmission and reception.

In Figs. 3a, 3b, and 3c, AEDs of the SV scenario for the three chosen $|N_N|$ values are shown. AEDs for the MV scenario are provided in Figs. 3d, 3e, and 3f. AEDs are the highest when $|N_S| = 1$, $\varphi = 0.25$, and $P_{\text{tx}} = 8$ W. AEDs for the MV scenario are a maximum of 46% lower than the AEDs for the SV scenario. The results reveal that the highest AEDs are 3.01 seconds and 1.92 seconds for the SV and the MV scenarios, respectively. On the contrary, the lowest AED is obtained as 0.52 seconds when $|N_S| = 25$, $\varphi = 0$, and $P_{\text{tx}} = 2$ W. Note that when $\varphi = 0$, AEDs for the SV and the MV scenarios are equivalent. When $|N_S|$ and P_{tx} are kept constant, AEDs extend as φ increases since packets need more time to circumvent the large void regions to reach the sink node(s). As φ increases from 0 to 0.25, the increment of AEDs is at most 150%. AEDs also increase as $|N_S|$ decreases for fixed φ and P_{tx} since the number of possible routing paths with low delays reduces as $|N_S|$ decreases. For a given $|N_S|$ and φ, AEDs rise as P_{tx} increases since sensor

nodes transmit their data to the nodes close to them to save energy for extending the network lifetime. Single-sink UWSNs have AEDs in 0.94–3.01 seconds. Multi-sink architectures can reduce the AEDs of single-sink architectures by at most 53%. Multi-sink architectures have AEDs in 0.52–1.92 seconds. Increasing $|N_N|$ has the advantage of creating many short routing paths with low delays, thus decreasing AEDs.

Figs. 4a, 4b, and 4c compare AETs for the SV scenario, while Figs. 4d, 4e, and 4f show AETs for the MV scenario for the three different network density options. The minimum AET is calculated as 96.05 mJ, and it is observed when $|N_S| = 25$, $P_{\text{tx}} = 2$ W, and $\varphi = 0$. For $|N_S| = 1$, $P_{\text{tx}} = 8$ W, and $\varphi = 0.25$, the maximum AETs are observed as 873.20 mJ and 812.18 mJ for the SV and MV scenarios, respectively. AETs for the SV and MV scenarios are identical when $\varphi = 0$. Void-free AETs (when $\varphi = 0$) rise at most 135% when $\varphi = 0.25$. The maximum difference of AETs between the SV and MV scenarios is obtained as 40%. AETs grow by increasing φ (for constant $|N_S|$ and P_{tx}), decreasing $|N_S|$ (for fixed φ and P_{tx}), or increasing P_{tx} (for constant $|N_S|$ and φ). Single-sink UWSNs have the minimum and the maximum AETs of 157 mJ and 873.20 mJ, respectively. On the other hand, multi-sink UWSNs have AETs in the interval of 96.05–690.98 mJ. Nevertheless, multi-sink UWSNs have at most 50% reduced AETs than single-sink UWSNs. An alternative way of reducing AETs is to consider a dense network by increasing $|N_N|$.

The assessment of AHC for the SV scenario is presented in Figs. 5a, 5b, and 5c. Furthermore, AHCs for the MV scenario are depicted in Figs. 5d, 5e, and 5f. AHCs are in the intervals of 4.88–10.58 and 4.88–10.33 for the SV and MV scenarios, respectively. The minimum AHC (which is 4.88) is observed when $|N_S| = 25$, $P_{\text{tx}} = 2$ W, and $\varphi = 0$. On the other hand, the maximum AHCs are obtained (for the two void region scenarios) when $|N_S| = 1$, $P_{\text{tx}} = 8$ W, and $\varphi = 0.25$. AHCs are indistinguishable when $\varphi = 0$. We observe a 16% maximum difference in AHCs for the SV and MV scenarios as φ grows. Our results show at most a 38% increment in AHCs as φ increases from 0 to 0.25. AHCs rise when φ is increased, P_{tx} is increased, or $|N_S|$ is decreased while the other parameters remain constant. Single-sink UWSNs have higher AHCs than multi-sink UWSNs. AHCs for the single-sink and the multi-sink UWSNs are in the intervals of 6.04–10.58 and 4.88–9.48, respectively. Nonetheless, for the multi-sink architectures, AHCs of the single-sink UWSNs can be reduced by at most 31%. Finally, the increment in $|N_N|$ results in AHCs being raised.

In Figs. 6a, 6b, and 6c, APLs are provided for the SV scenario, while Figs. 6d, 6e, and 6f show APLs for the MV scenario considering three $|N_N|$ values. The minimum APL is calculated as 185.48 dB (when $|N_S| = 25$, $P_{\text{tx}} = 2$ W, and $\varphi = 0$), and the maximum APLs are revealed as 946.94 dB and 622.77 dB for the SV and MV scenarios, respectively (when $|N_S| = 1$, $P_{\text{tx}} = 8$ W, and $\varphi = 0.25$). When the $\varphi = 0$, the APLs obtained in the SV and MV scenarios are the same. As φ increases from 0 to 0.25, the increase of APLs is at most 166%. Nevertheless, APLs of the SV scenario are at most 37% higher than APLs of the MV scenario. APLs increase φ rises or $|N_N|$, $|N_S|$, or P_{tx} decreases provided that the other two parameters are kept constant. Single-sink UWSNs have at most 53% greater APLs than multi-sink UWSNs such that APLs obtained for the single-sink and the multi-sink architectures are in 279.29–946.94 dB and 185.48–561.63 dB, respectively.

V. Conclusion

In this manuscript, we investigate the joint impact of communication void region size and the sink architecture type on UWSNs performance in terms of network lifetime, end-to-end delay, energy tax, hop count, and attenuation. The assessment is carried out for a large parameter space by using the optimal solutions of the developed ILP model that maximizes the UWSNs lifetime while bypassing the void regions available in the network. Our main conclusions are summarized as follows:

1) UWSNs lifetimes obtained without any void regions are shortened by more than half (up to 61%) if one-quarter of the network volume is considered as the void region. In this case, the other performance metrics (*i.e.*, AEDs, AETs, AHCs, and APLs) obtained for void-free UWSNs are increased by up to 1.6 times.
2) A large single void region has more catastrophic effects than multiple small void regions. Provided that the percent volume occupied by the void regions in the network is constant, UWSN lifetimes obtained with multiple void regions are at a maximum of 59% higher than the UWSNs lifetimes obtained with a single void region. AEDs, AETs, AHCs, and APLs obtained in the multi-void scenario are at most 46% less than those performance metrics obtained in the single void scenario.
3) It is recommended to utilize a multi-sink architecture instead of a single-sink architecture to alleviate the effects of the void region problem. Single-sink UWSN lifetimes can be prolonged at a minimum of 37% if a multi-sink architecture is used. Furthermore, multi-sink UWSNs have at most 53% reduced AEDs, AETs, AHCs, and APLs as opposed to the single-sink UWSNs.

References

[1] H. Nasir, N. Javaid, S. Mahmood, U. Qasim, Z. A. Khan, and F. Ahmed, "Distributed topology control protocols for underwater sensor networks," in *Proc. Int. Conf. Netw.-Based Inform. Syst. (NBiS)*, 2016, pp. 429–436.

[2] A. Sher, A. Khan, N. Javaid, S. Ahmed, M. Y. Aalsalem, and W. Z. Khan, "Void hole avoidance for reliable data delivery in IoT enabled underwater wireless sensor networks," *Sensors*, vol. 18, p. 3271, 2018.

[3] R. W. L. Coutinho, A. Boukerche, L. F. M. Vieira, and A. A. F. Loureiro, "GEDAR: Geographic and opportunistic routing protocol with depth adjustment for mobile underwater sensor network," in *Proc. IEEE Int. Conf. Commun. (ICC)*, 2014, pp. 251–256.

[4] S. M. Ghoreyshi, A. Shahrabi, and T. Boutaleb, "An opportunistic void avoidance routing protocol for underwater sensor networks," in *Proc. IEEE Int. Conf. Adv. Inform. Netw. Appl. (AINA)*, 2016, pp. 316–323.

[5] R. W. L. Coutinho, L. F. M. Vieira, and A. A. F. Loureiro, "DCR: Depth-controlled routing protocol for underwater sensor networks," in *Proc. IEEE Symp. Comput. Commun. (ISCC)*, 2013.

[6] S. M. Ghoreyshi, A. Shahrabi, and T. Boutaleb, "An inherently void avoidance routing protocol for underwater sensor networks," in *Proc. Int. Symp. Wirel. Commun. Syst. (ISWCS)*, 2015, pp. 361–365.

[7] R. W. L. Coutinho, A. Boukerche, L. F. M. Vieira, and A. A. F. Loureiro, "Geographic and opportunistic routing for underwater sensor networks," *IEEE Trans. Comput.*, vol. 65, no. 2, pp. 548–561, 2016.

[8] R. Mhemed, W. Phillips, F. Comeau, and N. Aslam, "Void avoiding opportunistic routing protocols for underwater wireless sensor networks: A survey," *Sensors*, vol. 22, no. 23, 2022.
[9] S. M. Ghoreyshi, A. Shahrabi, and T. Boutaleb, "A novel cooperative opportunistic routing scheme for underwater sensor networks," *Sensors*, vol. 16, no. 3, p. 297, 2016.
[10] R. W. L. Coutinho, A. Boukerche, L. F. M. Vieira, and A. A. F. Loureiro, "Local maximum routing recovery in underwater sensor networks: Performance and trade-offs," in *Proc. IEEE Int. Symp. Model. Anal. Simul. Comput. Telecommun. Syst.*, 2014, pp. 112–119.
[11] R. W. Coutinho, A. Boukerche, L. F. Vieira, and A. A. Loureiro, "A novel void node recovery paradigm for long-term underwater sensor networks," *Ad Hoc Netw.*, vol. 34, pp. 144–156, 2015.
[12] S. M. Ghoreyshi, A. Shahrabi, and T. Boutaleb, "Void-handling techniques for routing protocols in underwater sensor networks: Survey and challenges," *IEEE Commun. Surv. Tut.*, vol. 19, no. 2, pp. 800–827, 2017.
[13] D. Han, X. Du, and X. Liu, "CELR: Connectivity and energy aware layering routing protocol for uans," *IEEE Sens. J.*, vol. 21, no. 5, pp. 7046–7057, 2021.
[14] D. Shin, D. Hwang, and D. Kim, "DFR: An efficient directional flooding-based routing protocol in underwater sensor networks," *Wirel. Commun. and Mobile Comput.*, vol. 12, no. 17, pp. 1517–1527, 2012.
[15] Z. Wang, G. Han, H. Qin, S. Zhang, and Y. Sui, "An energy-aware and void-avoidable routing protocol for underwater sensor networks," *IEEE Access*, vol. 6, pp. 7792–7801, 2018.
[16] K. Hao, Y. Ding, C. Li, B. Wang, Y. Liu, X. Du, and C. Q. Wang, "An energy-efficient routing void repair method based on an autonomous underwater vehicle for UWSNs," *IEEE Sens. J.*, vol. 21, no. 4, pp. 5502–5511, 2021.
[17] S. M. Ghoreyshi, A. Shahrabi, and T. Boutaleb, "An underwater routing protocol with void detection and bypassing capability," in *Proc. IEEE Int. Conf. Adv. Inform. Netw. Appl. (AINA)*, 2017, pp. 530–537.
[18] Y. Noh, U. Lee, S. Lee, P. Wang, L. F. M. Vieira, J. Cui, M. Gerla, and K. Kim, "HydroCast: Pressure routing for underwater sensor networks," *IEEE Trans. Veh. Technol.*, vol. 65, no. 1, pp. 333–347, 2016.
[19] P. Nazareth and B. R. Chandavarkar, "Link and void aware routing protocol for underwater acoustic sensor networks," in *Proc. Int. Conf. Comput. Commun. Netw. Technol. (ICCCNT)*, 2021, pp. 1–6.
[20] J. Chen, X. Wu, and G. Chen, "REBAR: A reliable and energy balanced routing algorithm for UWSNs," in *Proc. Int. Conf. Grid Coop. Comput.*, 2008, pp. 349–355.
[21] Y. Zhang, Z. Zhang, L. Chen, and X. Wang, "Reinforcement learning-based opportunistic routing protocol for underwater acoustic sensor networks," *IEEE Trans. Veh. Technol.*, vol. 70, no. 3, pp. 2756–2770, 2021.
[22] M. Ismail, M. Islam, I. Ahmad, F. A. Khan, A. B. Qazi, Z. H. Khan, Z. Wadud, and M. Al-Rakhami, "Reliable path selection and opportunistic routing protocol for underwater wireless sensor networks," *IEEE Access*, vol. 8, pp. 100 346–100 364, 2020.
[23] Y. Noh, U. Lee, P. Wang, B. S. C. Choi, and M. Gerla, "VAPR: Void-aware pressure routing for underwater sensor networks," *IEEE Trans. Mobile Comput.*, vol. 12, no. 5, pp. 895–908, 2013.
[24] P. Xie, J.-H. Cui, and L. Lao, "VBF: Vector-based forwarding protocol for underwater sensor networks," in *Proc. Int. IFIP-TC6 NETWORKING*, 2006, p. 1216–1221.
[25] P. Xie, Z. Zhou, Z. Peng, J.-H. Cui, and Z. Shi, "Void avoidance in three-dimensional mobile underwater sensor networks," in *Proc. Int. Conf. Wirel. Algo. Syst. Appl. (WASA)*, 2009, pp. 305–314.
[26] H. Yu, N. Yao, and J. Liu, "An adaptive routing protocol in underwater sparse acoustic sensor networks," *Ad Hoc Netw.*, vol. 34, pp. 121–143, 2015.
[27] S. Basagni, C. Petrioli, R. Petroccia, and D. Spaccini, "CARP: a channel-aware routing protocol for underwater acoustic wireless networks," *Ad Hoc Netw.*, vol. 34, pp. 92–104, 2015.
[28] J. M. Jornet, M. Stojanovic, and M. Zorzi, "Focused beam routing protocol for underwater acoustic networks," in *Proc. ACM Int. Workshop Underw. Netw.*, 2008, p. 75–82.
[29] A. Khan, I. Ahmedy, M. H. Anisi, N. Javaid, I. Ali, N. Khan, M. Alsaqer, and H. Mahmood, "A localization-free interference and energy holes minimization routing for underwater wireless sensor networks," *Sensors*, vol. 18, no. 1, p. 165, 2018.
[30] Z. Rahman, F. Hashim, M. F. A. Rasid, M. Othman, and K. Ali Alezabi, "Normalized advancement based totally opportunistic routing algorithm with void detection and avoiding mechanism for underwater wireless sensor network," *IEEE Access*, vol. 8, pp. 67 484–67 500, 2020.
[31] R. W. Coutinho, L. F. Vieira, and A. A. Loureiro, "Movement assisted-topology control and geographic routing protocol for underwater sensor networks," in *Proc. ACM Int. Conf. Model. Anal. Simul. Wirel. Mobile Syst. (MSWiM)*, 2013, p. 189–196.
[32] M. Jouhari, K. Ibrahimi, M. Benattou, and A. Kobbane, "New greedy forwarding strategy for UWSNs geographic routing protocols," in *Proc. Int. Wirel. Commun. Mobile Comput. Conf. (IWCMC)*, 2016, pp. 388–393.
[33] Z. Jin, Q. Zhao, and Y. Luo, "Routing void prediction and repairing in AUV-assisted underwater acoustic sensor networks," *IEEE Access*, vol. 8, pp. 54 200–54 212, 2020.
[34] H. Yu, N. Yao, T. Wang, G. Li, Z. Gao, and G. Tan, "WDFAD-DBR: Weighting depth and forwarding area division DBR routing protocol for UASNs," *Ad Hoc Netw.*, vol. 37, pp. 256–282, 2016.
[35] G. Latif, N. Javaid, A. Sher, M. Khan, T. Hameed, and W. Abbas, "An efficient routing algorithm for void hole avoidance in underwater wireless sensor networks," in *Proc. IEEE Int. Conf. Adv. Inform. Netw. Appl. (AINA)*, 2018, pp. 305–310.
[36] M. Awais, I. Ali, T. A. Alghamdi, M. Ramzan, M. Tahir, M. Akbar, and N. Javaid, "Towards void hole alleviation: Enhanced geographic and opportunistic routing protocols in harsh underwater WSNs," *IEEE Access*, vol. 8, pp. 96 592–96 605, 2020.
[37] M. Jouhari, K. Ibrahimi, and M. Benattou, "Topology control through depth adjustment and transmission power control for UWSN routing protocols," in *Proc. Int. Conf. Wirel. Netw. Mobile Commun. (WINCOM)*, 2015, pp. 1–5.
[38] K. Latif, N. Javaid, A. Ahmad, Z. A. Khan, N. Alrajeh, and M. I. Khan, "On energy hole and coverage hole avoidance in underwater wireless sensor networks," *IEEE Sens. J.*, vol. 16, no. 11, pp. 4431–4442, 2016.
[39] R. W. Coutinho, A. Boukerche, L. F. Vieira, and A. A. Loureiro, "Performance modeling and analysis of void-handling methodologies in underwater wireless sensor networks," *Comput. Netw.*, vol. 126, pp. 1–14, 2017.
[40] D. Zhang and E. Dong, "A virtual coordinate-based bypassing void routing for wireless sensor networks," *IEEE Sens. J.*, vol. 15, no. 7, pp. 3853–3862, 2015.
[41] M. Stojanovic, "On the relationship between capacity and distance in an underwater acoustic communication channel," in *Proc. ACM Int. Workshop Underw. Netw.*, 2006, p. 41–47.
[42] S. Ergen and P. Varaiya, "On multi-hop routing for energy efficiency," *IEEE Commun. Lett.*, vol. 9, no. 10, pp. 880–881, 2005.
[43] P. Bourke, "Intersection of a Line and a Sphere (or circle)," 1992. [Online]. Available: http://paulbourke.net/geometry/circlesphere/

Huseyin Ugur Yildiz (Senior Member, IEEE) received B.S. degree from Bilkent University, Ankara, Turkey, in 2009; M.S. and Ph.D. degrees from TOBB University of Economics and Technology, Ankara, in 2013 and 2016, respectively, all in electrical and electronics engineering. He is currently an Associate Professor and the Chair of the Department of Electrical and Electronics Engineering at TED University, Ankara. His research focuses on the applications of optimization techniques for wireless communications, ad hoc networks, underwater wireless sensor networks, and smart grids.